Supplementary Materials

An Observation-Based Methodology and Application for Future Atmosphere Secondary Pollution Control via an Atmospheric Oxidation Capacity Path Tracing Approach

Ke Yue a,b, Yulong Yan a,b,*, Yueyuan Niu c, Jiaqi Dong a,b, Chao Yang d, Yongqian Zhou a,b, Danning Wang a,b, Junjie Li a,b, Zhen Li a,b, Lin Peng a,b,*

^a Engineering Research Center of Clean and Low-carbon Technology for Intelligent

Transportation, Ministry of Education, School of Environment, Beijing Jiaotong University,

Beijing 100044, China

b School of Environment, Beijing Jiaotong University, Beijing 100044, China
c Flight College, Shandong University of Aeronautics, Binzhou, Shandong, 256600, China
d Shanxi Climate Center, Taiyuan, Shanxi 030006, China

- * Corresponding author, E-mail: yanyulong@bitu.edu.cn
- * Corresponding author, E-mail: penglin6611@163.com

Text S1

Changzhi is located in the southeast of Shanxi Province, with geographical coordinates of 113.123405 E and 36.160912 N. As a typical industrial city of China, the industrial structure of Changzhi City is dominated by coal mining, washing, power and thermal power production (Czmg, 2022). The coal industry accounts for more than 70% of the industrial economy, and nearly 90% of the energy structure is coal (Czmg, 2022). The proportion of coal consumption in high energy consuming industries reached 87.62% in the first three quarters of 2023 (Czmbs, 2023). Meanwhile, the main heavy industries

in Changzhi are coking and steel, as is typical for an industrial city (Niu et al., 2024a). 6.2 million tons of steel and 16.4 million tons of coke have been produced by Changzhi in 2023, that outpacing the majority of cities in Shanxi Province (Czmbs, 2023). Therefore, this study selected Changzhi as a representative of typical industrial city.

The sampling site was located on a rooftop of Residential buildings at the QingHuaZhan of Changzhi, representing an urban environment without nearby large industrial pollution sources, adjacent to the main traffic lanes and surrounded by residential areas. Sampling period from June 2 to June 30, 2021. The sampling rate is 2 hours, and a total of 12 consecutive samples are collected in one day.

Text S2

Briefly, the samples were pumped in to the liquid-nitrogen cryogenic trap (at -160 $^{\circ}$ C), Tenax-TA trap (at -40 $^{\circ}$ C) and cryofocus trap (at -170 $^{\circ}$ C) in sequence, to concentrate volatile organic compounds (VOCs) and remove H₂O and CO₂. Then, the cryofocus trap was rapidly heated and VOCs were transferred to the gas chromatography-mass selective detector (GC-MSD) system. A DB-1 capillary column (60 m × 0.32 mm × 1.0 mm, Agilent Technologies, USA) was used with helium as carrier gas. The gas chromatography (GC) oven temperature was programmed to be initially at -50 $^{\circ}$ C, holding for 3 min. Then the temperature increased to 10 $^{\circ}$ C at 15 $^{\circ}$ C/min, and to 120 $^{\circ}$ C at 5 $^{\circ}$ C/min, then to 250 $^{\circ}$ C at 10 $^{\circ}$ C/min, and finally holding for 10 min. The mass selective detector (MSD) was used in selected ion monitoring (SIM) mode and the ionization method was electron impacting (EI, 70 eV) with the source temperature was 220 $^{\circ}$ C.

Text S3

For alkanes, the recommended temperature-dependent expression is a

three-parameter expression is used Eq.(S1) (Atkinson, 2003). For alkenes, alkynes, and aromatics is used Eq. (S2) (Atkinson, 2003).

$$k_{OH} = AT^n e^{-B/T} \tag{S1}$$

$$k_{OH} = Ae^{-B/T} (S2)$$

where A is the Arrhenius constant (cm 3 · molecule $^{-1}$ · s $^{-1}$); B is the ratio of the apparent activation energy (Ea) to the molar gas constant (R) (K); and n is a coefficient, generally n=2. T is the temperature (K).

The photochemical age or time that VOCi's reaction with OH radicals $\triangle t$ was calculated by Eq. (S3) to (S5) (Niu et al., 2024c).

$$\Delta t = \min (t_d(or t_a), t_r)$$
 (S3)

$$t_r = \frac{\overline{D}}{r} \times p \tag{S4}$$

$$p = \frac{\overline{WD}}{WD_{all}} \times 100\%$$
 (S5)

Where t_d is monthly daytime duration, and is identified as 13 hour in this study, which is applicable to the calculation of species except isoprene; t_d is the photochemical age of isoprene reacts completely, which is applicable to the calculation of isoprene; t_r is the residence time of species in the transport from source to receptor; \overline{D} is the average distance between pollution source and observation site (m); p is a weighting function based on wind speed, wind direction; \overline{WD} is the measured monthly averaged dominant wind direction; WD_{all} is averaged monthly wind direction. The detail of this method refer to the study (Wang et al., 2022).

Text S4

The calculation theory of PMF is shown in Eq. (S6). The uncertainty of the sample data was calculated using Eq. (S7).

$$C_{ik} = \sum_{j=1}^{p} A_{ij} B_{jk} + \epsilon_{ik} (i = 1, 2, ..., n)$$
 (S6)

where Cik represents the concentration of species i in sample k; j and p

represent the pollution source j and the number of pollution sources; A_{ij} and B_{jk} represent the source profile and source contribution, respectively; and ϵ_{ik} represents the residue factor.

$$U = \begin{cases} \sqrt{(E \cdot c)^2 + M^2 (c > M)} \\ \frac{5}{6} M (c \le M) \end{cases}$$
 (S7)

where c was the concentration of species. E was the error ratio (0.2). M was the detection limit of the species. In this model, the objective function Q is solved with an iterative minimization algorithm, and the Q value must be as small as possible. The objective function was defined in Eq. (S8).

$$Q = \sum_{i}^{m} \sum_{k}^{n} \left(\frac{\varepsilon_{ik}}{\sigma_{ik}}\right)^{2}$$
 (S8)

where σ_{ik} represents the uncertainty bias of the sample. m and n represent the number of species and the number of samples, respectively.

Text S5

The concentration of Isoprene, anthropogenic alkene, oxygenated VOCs, aromatics, alkane, alkynes and haloalkane from InVOCs were higher than MVOCs 34.8%, 29.9%, 29.7%, 2.5%, 1.4% and 1.2%, respectively.

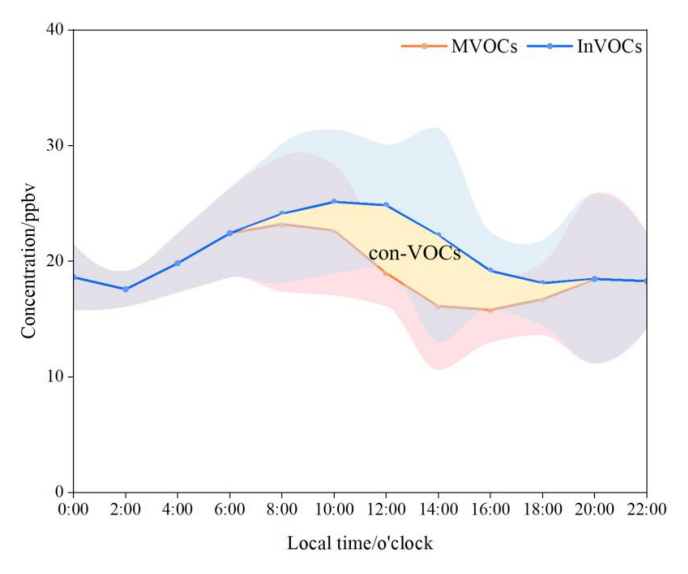


Fig. S1. Diurnal variations in concentrations of InVOCs and MVOCs

The net O_3 formation rate (Net (O_3)) during the observation period was simulated by the F0AM model. These simulations were utilized to characterize O_3 formation processes, quantify formation potential of O_3 , and conduct sensitivity analyses with precursors (InVOCs and NO_x). The calculations for Net (O_3) were shown in Eqs. (S9) - (S11), respectively.

$$\begin{split} \text{Net}(O_3) &= \text{P}(O_3) - \text{L}(O_3) \\ \text{(S9)} \\ \text{P}(O_3) &= \text{k}_{\text{HO}_2 + \text{NO}}[\text{HO}_2][\text{NO}] + \text{k}_{\text{RO}_2 + \text{NO}}[\text{RO}_2][\text{NO}] \\ \text{L}(O_3) &= \text{k}_{\text{O}_3 + \text{OH}}[O_3][\text{OH}] + \text{k}_{\text{O}_3 + \text{HO}_2}[O_3][\text{HO}_2] + \text{k}_{\text{O}_3 + \text{alkenes}}[O_3][\text{alkenes}] + \\ &\qquad \qquad \text{k}_{\text{NO}_2 + \text{OH}}[\text{NO}_2][\text{OH}] + \text{k}_{\text{O}(^1\text{D}) + \text{H}_2\text{O}}[\text{O}(^1\text{D})][\text{H}_2\text{O}] \end{split} \tag{S11}$$

Where P(O₃) and L(O₃) are the production and loss rates of O₃, respectively. [HO₂], [RO₂], [NO], [O₃], [OH], [HO₂], [alkenes], [NO₂], [O1D] and [H₂O] are the concentration of the compounds and free radicals, respectively. $k_{\rm HO_2+NO}$, $k_{\rm RO_2+NO}$, $k_{\rm O_3+OH}$, and $k_{\rm O_1^1D}$ +H₂O are the reaction rates.

We applied F0AM model to analyzed the production and loss pathways of O3, to study the atmospheric photochemical reaction mechanism during different periods (Fig. S2.). The maximum net (O₃) was 28.2 ppbv·h⁻¹ in pollution period, which higher than clean period 90.5%. Research shows that InVOCs can react with OH· and produce peroxyl radicals (HO₂·· and RO₂··), consuming NO and finally causing net O3 formation (Wei et al., 2023; Yang et al., 2024; Okazaki et al., 2021). HO₂· + NO was the dominated reaction of O₃ production, which the highest rate in pollution and clean period were 18.6 ppbv·h⁻¹ and 10.0 ppbv·h⁻¹, respectively. NO + RO₂· was another dominated reaction of O₃ production, the reaction of CH3O2 and BUT2OLO2 with NO were important, which was

productid from the reaction of CH4 and TBUT2ENE (name from MCM) with OH·, respectively. O_3 + alkene was the dominated reaction of O_3 loss, which accounting for 41.8% of the O_3 loss during the study period (Fig. S3.). Compared with other cities, the maximum net (O_3) of Changzhi during the study period (21.5 ppbv·h⁻¹) was higher than Beijing (approx. 13 ppbv·h⁻¹) (Jia et al., 2023), Lanzhou (approx. 17 ppbv·h⁻¹) (Liu et al., 2021), and the background site of China (4.1 ppbv·h⁻¹) (Li et al., 2021). The higher maximum net (O_3) may be due to higher reactions between NO and free radicals (HO₂·, RO₂·, etc.), including precursor of VOCs species which generate RO₂·. According with the atmospheric photochemical mechanism to reduce the precursor concentration of emission sources is important, which to relieve O_3 pollution.

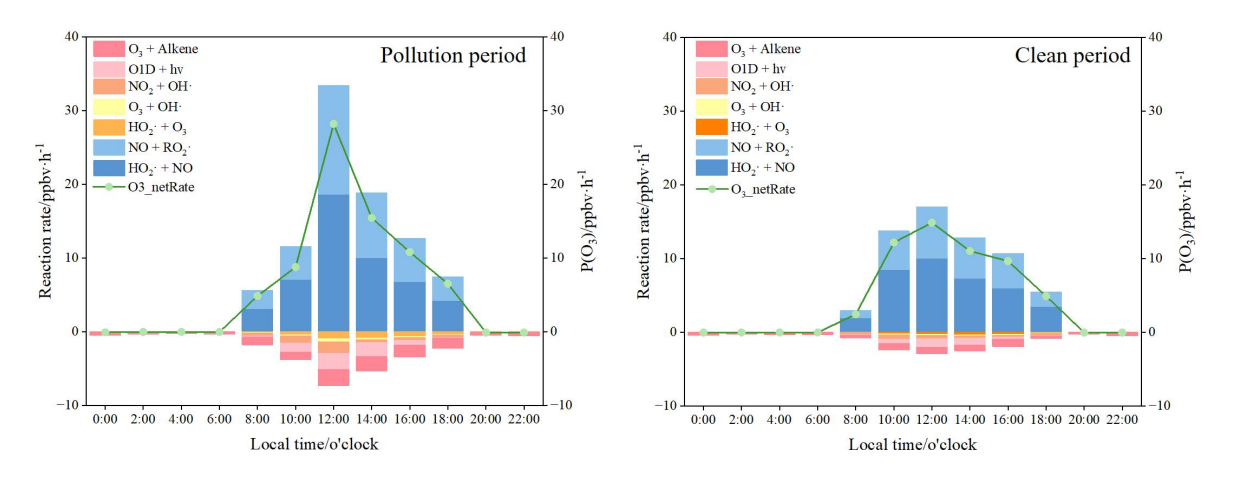


Fig. S2. Diurnal patterns of O₃ production and loss rates simulated

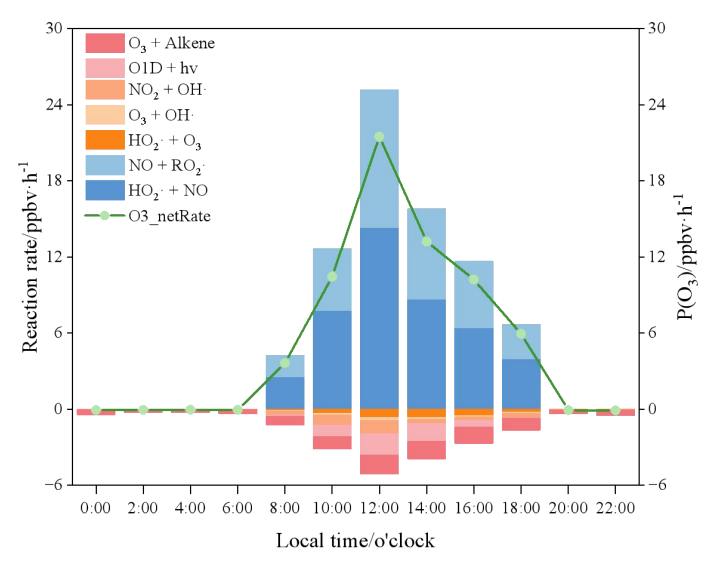


Fig.S3 Diurnal patterns of O₃ production and loss rates simulated

Further analysis was conducted to investigate the correlations between AOC and both con-VOCs and key free radicals, particularly OH· radicals, which were identified as significant contributors to AOC through observed linear relationships. The linear relationships between AOC and OH· radicals was the strongest, with a fitting degree of R^2 =0.77, which is higher than con-VOCs (R^2 =0.59) and HO_2 · (R^2 =0.40). These findings of correlation verification further corroborated the significantly greater contribution of OH· to AOC (Fig. S4.).

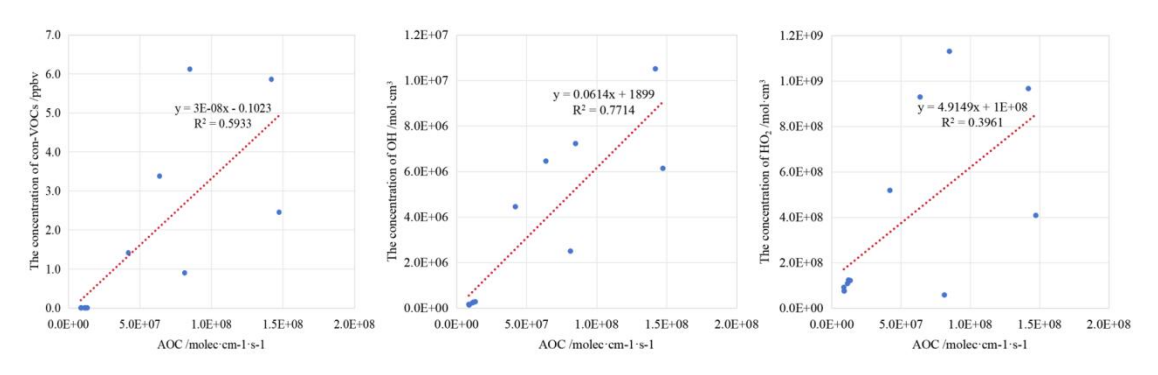


Fig. S4 The linear relationships between AOC and con-VOCs, OH and HO₂.

Text S8

Factor 1 was characterized by high percentages of ethane (43.0%), propane (59.5%), isopentane (59.2%), n-pentane (33.2%), 2,3-dimethyl-butane (44.3%),

ethylene (33.6%), propylene (34.1%), 1-pentene (32.3%), toluene (26.2%), acrolein (37.0%) and propanal (34.8%). C4-C6 alkanes and alkenes are both the main components of gasoline, some aromatics are the main species of gasoline vehicle emission (Huang et al., 2011; Gentner et al., 2013; Zhang et al., 2018). Therefore, Factor 1 was considered as gasoline vehicle emission. Factor 2 was characterized by high percentages of 1-butene (39.3%), trans-2-butene (36.3%), 1,3-Butadiene (35.8%), ethyl-benzene (37.4%), m/p-Xylene (25.2%). These were the important species of steel and coking industries (Xu et al., 2021). (Jiun-Horng et al., 2008) found that some aromatic compounds (e.g., m/p-xylene and ethyl-benzene) were the predominant VOCs species of the iron and steel industry, constituting 45%~70% of the total VOCs concentrations. Moreover, the 1,2-dichloroethane (59.4%), 1,2-dichloropane (46.3%) and other chlorinated compounds come from the chemical industry (Bartkowiak et al., 2006). Therefore, Factor 2 was identified as industrial process. Factor 3 was identified by high percentages of styrene (32.6%), isopropyl benzene (47.3%), n-propyl benzene (48.1%), 1,2,4-trimethyl benzene (31.4%), 1,2,3-trimethyl benzene (53.9%), chloromethane (30.4%) and methylene-chloride (49.3%). These species were related to the use of solvents in painting, coating, synthetic fragrances and cleaning agents (Hui et al., 2018; Wu and Xie, 2017). Therefore, Factor 3 was considered as solvent utilization. Factor 4 had high percentages of ethane (26.4%), ethylene (19.2%), acetylene (45.7%), benzene (56.4%). These species are the tracers of coal combustion (Niu et al., 2021). Therefore, Factor 4 was considered to represent a source of combustion source. Factor 5 had higher proportion of isopentane (25.4%), 2-methyl-heptane (35.4%), 3-methyl-heptane (39.5%), n-hexane (39.8%), 3-methyl-hexane (46.1%), n-undecane (45.8%), m/p-xylene (38.4%) and NO_x (42.8%). These species were the main pollutants of diesel vehicle emission (Wu and Xie, 2017). Therefore, Factor 5 was attributed to diesel vehicle emission. Factors 6 was dominated by higher contribution of isoprene, accounting for 91.2% of the total InVOCs concentrations. As isoprene is an

indicator of biogenic emission, Factor 2 was attributed to biogenic source.

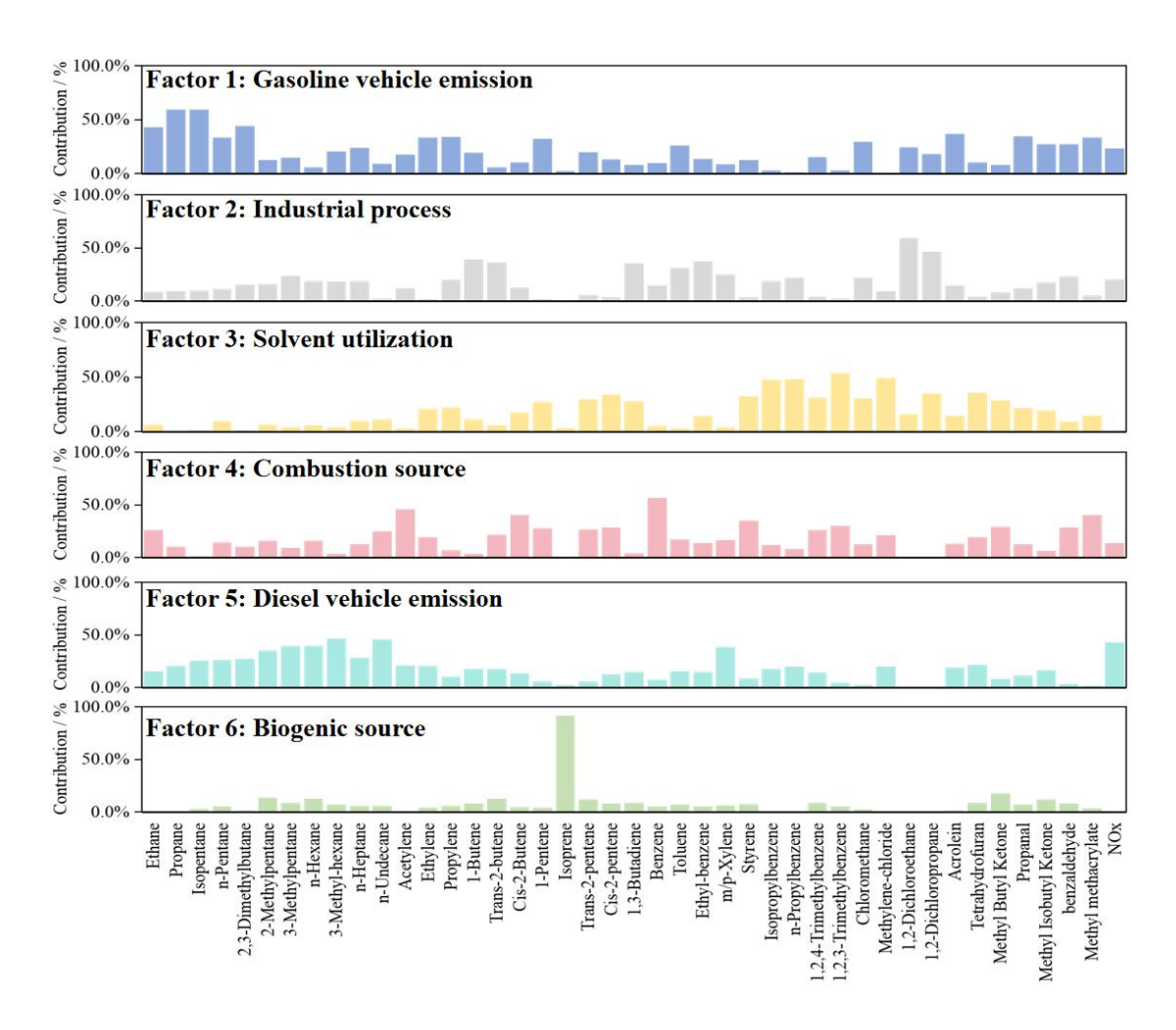


Fig.S4 Source contribution from the PMF model.

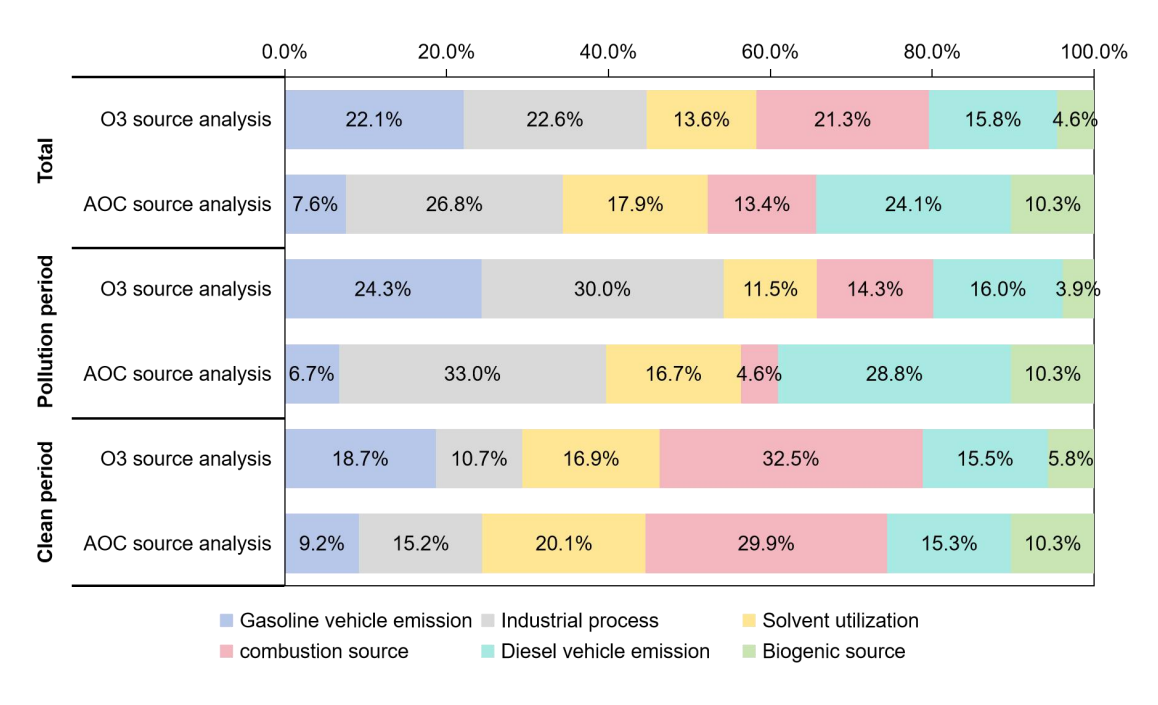


Fig.S5 Source contribution of O₃ and AOC.

The typical secondary pollutants include not only O₃, but also Secondary Organic Aerosols (SOA), which is an important secondary component of PM_{2.5}, with complex formation processes and significant governance challenges (Dou et al., 2024). The self-reaction rate between peroxy radicals (Self-Rxns) is typically used to characterize the formation potential of SOA, which include three types of reactions between peroxy radicals, i.e., RO₂·+RO₂·, RO₂·+HO₂·, and HO₂·+HO₂· (Lyu et al., 2022). In this study, we used F0AM-MCMv3.3.1 to investigate the nonlinear relationships between precursors (VOCs and NO_x) and self-rxns. HO₂·+HO₂· represents the reaction of HO₂· with itself that leads to the formation of hydrogen peroxide. RO2·+HO2· is the set of reactions between HO₂· and all individual RO₂·. RO₂·+RO₂· represents the set of reactions between specific RO₂· and all individual RO₂·, which are summed up as a single reaction with RO₂ "pool". The sum of all these reactions is the overall reaction rate of self-rxns (as shown in Eqs.S12 (Niu et al., 2024b)). $self - rxns = k_{RO_2 + RO_2}[RO_2][RO_2] + k_{HO_2 + HO_2}[HO_2][HO_2] + k_{HO_2 + RO_2}[HO_2][RO_2]$ (S12) Where [HO₂] and [RO₂] are the concentrations of the free radicals. $k_{RO_2+RO_2}$, $k_{RO_2+RO_2}\,$ and $\,k_{RO_2+RO_2}\,$ are the reaction rates.

The daytime (8 -18 o'clock) RIR values of O_3 and AOC precursors during the sampling period were analyzed in this study (Fig. S6). Overall, throughout the sampling period, decreased O_3 consistently yielded positive RIR values for precursors. NO_x exhibited the highest sensitivity to O_3 (RIR, 0.64), followed by InVOCs (RIR, 0.42), with alkene being the most sensitive InVOCs component. For AOC, the NO_x also exhibited the highest sensitivity (RIR, 0.55), followed by alkene (RIR, 0.29), which have higher sensitive than InVOCs (RIR, 0.27). These findings indicate that targeted control of alkenes and NO_x is critical to effectively mitigate AOC and O_3 pollution.

Meanwhile, taking O_3 pollution as an example, NO_x exhibited the highest sensitivity both during the pollution and clean period (RIR, 0.59 and 0.45, respectively), consistently surpassing InVOCs (RIR, 0.45 and 0.38, respectively). Notably, InVOCs sensitivity was higher during pollution period than in clean periods, while NO_x sensitivity showed the opposite trend. Alkene dominated sensitivity among InVOCs in both pollution (0.28) and clean (0.31) periods.

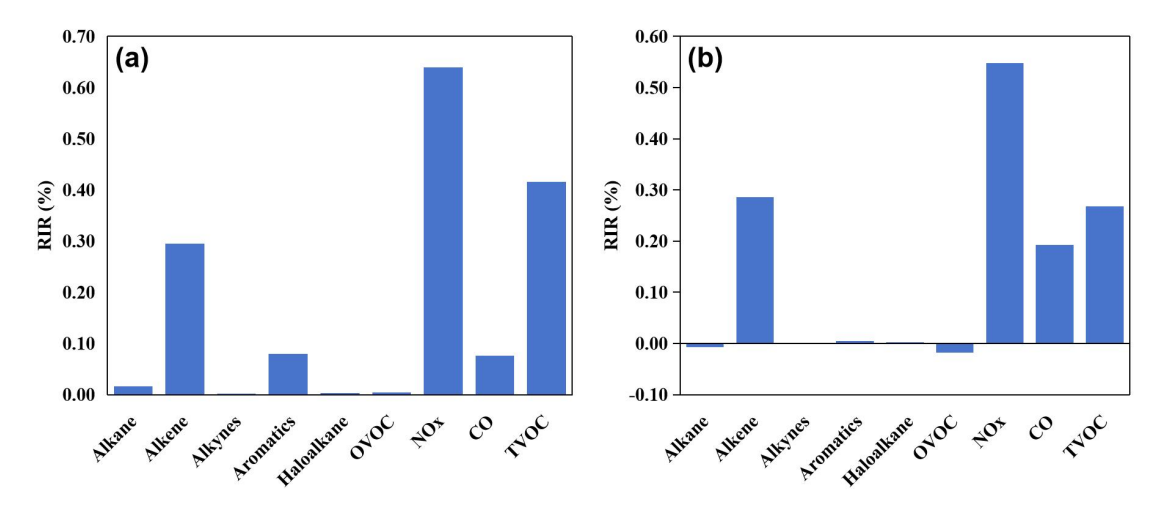


Fig.S6 Daytime (8 -18 o'clock) relative incremental reactivity (RIR) of O₃ (a) and AOC

(b) precursors during the sampling period

Fig. S7. shows the diurnal patterns of O₃ precursors sensitivities across sampling episodes. During pollution periods, O₃ formation exhibited the highest sensitivity to InVOCs, particularly alkene, between 8 - 10o'clock, while NO_x sensitivity remained negative due to O₃-NO_x titration effects (Liu et al., 1987). This aligns with higher AOC contributions from O₃+NO₂ in morning of pollution period (Fig. 2.). From 10 - 18o'clock of pollution period, O₃ was controlled by VOCs and NOx, with NOx sensitivity (peaking at 1.13 during 14 -16o'clock) surpassing InVOCs. In clean period, peak alkene sensitivity occurred earlier (6 - 8o'clock), followed by InVOCs-NO_x co-dominance from (10 - 18o'clock). RIR analysis highlights the necessity of phased control strategies for O₃ precursors, emphasizing NO_x's critical role in industrial cities (Xu et al., 2022). Excepted the vehicular and combustion source emissions, heavy industries (e.g., coking, steel, cement) significantly contribute to NO_x (Li et al., 2023). Thus, coordinated InVOCs and NO_x mitigation is imperative in industrial urban transition zones, where O₃ formation exhibits dual sensitivity (Dunker, 2015). However, given the complex nature of InVOCs sources, it is most critical to achieve emission reductions of key species and sources influencing atmospheric oxidation.

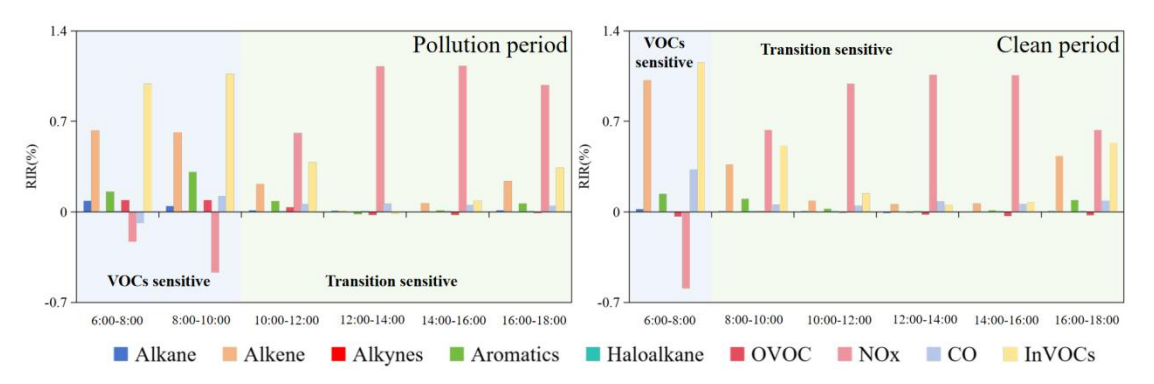


Fig. S7. Diurnal patterns of RIR simulated in pollution and clean period

References

- Atkinson, R.: Kinetics of the gas-phase reactions of OH radicals with alkanes and cycloalkanes, Atmos. Chem. Phys., 3, 2233-2307, 10.5194/acp-3-2233-2003, 2003.
- Bartkowiak, M., Lewandowski, G., Milchert, E., and Pełech, R.: Optimization of 1,2-Diaminopropane Preparation by the Ammonolysis of Waste 1,2-Dichloropropane, Ind. Eng. Chem. Res., 45, 5681-5687, 10.1021/ie051134u, 2006.
- Changzhi Municipal Bureau of Statistics: https://www.tjj.changzhi.gov.cn, last
- Changzhi Municipal Government: https://www.changzhi.gov.cn/, last
- Dou, X., Yu, S., Li, J., Sun, Y., Song, Z., Yao, N., and Li, P.: The WRF-CMAQ Simulation of a Complex Pollution Episode with High-Level O3 and PM2.5 over the North China Plain: Pollution Characteristics and Causes, Atmosphere., 15, 198, 2024.
- Dunker, A. M.: Path-integral method for the source apportionment of photochemical pollutants, Geoscientific Model Development., 8, 1763-1773, 10.5194/gmd-8-1763-2015, 2015.
- Gentner, D. R., Worton, D. R., Isaacman, G., Davis, L. C., Dallmann, T. R., Wood, E. C., Herndon, S. C., Goldstein, A. H., and Harley, R. A.: Chemical Composition of Gas-Phase Organic Carbon Emissions from Motor Vehicles and Implications for Ozone Production, Environ. Sci. Technol., 47, 11837-11848, 10.1021/es401470e, 2013.
- Huang, C., Chen, C. H., Li, L., Cheng, Z., Wang, H. L., Huang, H. Y., Streets, D. G., Wang, Y. J., Zhang, G. F., and Chen, Y. R.: Emission inventory of anthropogenic air pollutants and VOC species in the Yangtze River Delta region, China, Atmos. Chem. Phys., 11, 4105-4120, 10.5194/acp-11-4105-2011, 2011.
- Hui, L. R., Liu, X. G., Tan, Q. W., Feng, M., An, J. L., Qu, Y., Zhang, Y. H., and Jiang, M. Q.: Characteristics, source apportionment and contribution of VOCs to ozone formation in Wuhan, Central China, Atmos. Environ., 192, 55-71, 10.1016/j.atmosenv.2018.08.042, 2018.
- Jia, C. H., Tong, S. R., Zhang, X. R., Li, F. J., Zhang, W. Q., Li, W. R., Wang, Z., Zhang, G., Tang, G. Q., Liu, Z. R., and Ge, M. F.: Atmospheric oxidizing capacity in autumn Beijing: Analysis of the O3 and PM2.5 episodes based on observation-based model, Journal of Environmental Sciences., 124, 557-569, 10.1016/j.jes.2021.11.020, 2023.
- Jiun-Horng, T., Kuo-Hsiung, L., Chih-Yu, C., Nina, L., Sen-Yi, M., and Hung-Lung, C.: Volatile organic compound constituents from an integrated iron and steel facility, J. Hazard. Mater., 157, 569-578, 10.1016/j.jhazmat.2008.01.022, 2008.
- Li, T., Li, J., Sun, Z., Jiang, H., Tian, C., and Zhang, G.: High contribution of anthropogenic combustion sources to atmospheric inorganic reactive nitrogen in South China evidenced by isotopes, Atmos. Chem. Phys., 23, 6395-6407, 10.5194/acp-23-6395-2023, 2023.
- Li, Y., Gao, R., Xue, L., Wu, Z., Yang, X., Gao, J., Ren, L., Li, H., Ren, Y., Li, G., Li, C., Yan, Z., Hu, M., Zhang, Q., and Xu, Y.: Ambient volatile organic compounds at Wudang Mountain in Central China: Characteristics, sources and implications to ozone formation, Atmospheric Research., 250, 105359, https://doi.org/10.1016/j.atmosres.2020.105359, 2021.
- Liu, S. C., Trainer, M., Fehsenfeld, F. C., Parrish, D. D., Williams, E. J., Fahey, D. W., Hubler, G., and Murphy, P. C.: OZONE PRODUCTION IN THE RURAL TROPOSPHERE AND THE IMPLICATIONS FOR REGIONAL AND GLOBAL OZONE DISTRIBUTIONS, Journal of Geophysical Research-Atmospheres., 92, 4191-4207, 10.1029/JD092iD04p04191,

1987.

- Liu, X. F., Guo, H., Zeng, L. W., Lyu, X., Wang, Y., Zeren, Y. Z., Yang, J., Zhang, L. Y., Zhao, S. Z., Li, J., and Zhang, G.: Photochemical ozone pollution in five Chinese megacities in summer 2018, Sci. Total Environ., 801, 13, 10.1016/j.scitotenv.2021.149603, 2021.
- Lyu, X., Guo, H., Zou, Q. L., Li, K., Xiong, E. Y., Zhou, B. N., Guo, P. W., Jiang, F., and Tian, X. D.: Evidence for Reducing Volatile Organic Compounds to Improve Air Quality from Concurrent Observations and In Situ Simulations at 10 Stations in Eastern China, Environ. Sci. Technol., 9, 10.1021/acs.est.2c04340, 2022.
- Niu, Y., Yan, Y., Dong, J., Yue, K., Duan, X., Hu, D., Li, J., and Peng, L.: Evidence for sustainably reducing secondary pollutants in a typical industrial city in China: Co-benefit from controlling sources with high reduction potential beyond industrial process, J. Hazard. Mater., 478, 135556, 10.1016/j.jhazmat.2024.135556, 2024a.
- Niu, Y. Y., Yan, Y. L., Dong, J. Q., Yue, K., Duan, X. L., Hu, D. M., Li, J. J., and Peng, L.: Evidence for sustainably reducing secondary pollutants in a typical industrial city in China: Co-benefit from controlling sources with high reduction potential beyond industrial process, J. Hazard. Mater., 478, 10, 10.1016/j.jhazmat.2024.135556, 2024b.
- Niu, Y. Y., Yan, Y. L., Li, J., Liu, P., Liu, Z. C., Hu, D. M., Peng, L., and Wu, J.: Establishment and verification of anthropogenic volatile organic compound emission inventory in a typical coal resource-based city*, Environ. Pollut., 288, 9, 10.1016/j.envpol.2021.117794, 2021.
- Niu, Y. Y., Yan, Y. L., Xing, Y. R., Duan, X. L., Yue, K., Dong, J. Q., Hu, D. M., Wang, Y. H., and Peng, L.: Analyzing ozone formation sensitivity in a typical industrial city in China: Implications for effective source control in the chemical transition regime, Sci. Total Environ., 919, 10, 10.1016/j.scitotenv.2024.170559, 2024c.
- Okazaki, Y., Ito, L., and Tokai, A.: Health Risk of Increased O3 Concentration Based on Regional Emission Characteristics under the Unusual State of the COVID-19 Pandemic, Atmosphere., 12, 335, 2021.
- Wang, Z. Y., Shi, Z. B., Wang, F., Liang, W. Q., Shi, G. L., Wang, W. C., Chen, D., Liang, D. N., Feng, Y. C., and Russell, A. G.: Implications for ozone control by understanding the survivor bias in observed ozone-volatile organic compounds system, Npj Climate and Atmospheric Science., 5, 9, 10.1038/s41612-022-00261-7, 2022.
- Wei, N., Zhao, W., Yao, Y., Wang, H., Liu, Z., Xu, X., Rahman, M., Zhang, C., Fittschen, C., and Zhang, W.: Peroxy radical chemistry during ozone photochemical pollution season at a suburban site in the boundary of Jiangsu–Anhui–Shandong–Henan region, China, Sci. Total Environ., 904, 166355, 10.1016/j.scitotenv.2023.166355, 2023.
- Wu, R. R. and Xie, S. D.: Spatial Distribution of Ozone Formation in China Derived from Emissions of Speciated Volatile Organic Compounds, Environ. Sci. Technol., 51, 2574-2583, 10.1021/acs.est.6b03634, 2017.
- Xu, C. X., He, X. J., Sun, S. D., Bo, Y., Cui, Z. Q., Zhang, Z. C., and Dong, H.: Sensitivity of Ozone Formation in Summer in Jinan Using Observation-Based Model, #N/A, 13, 18, 10.3390/atmos13122024, 2022.
- Xu, Y., Yu, H. L., Yan, Y. L., Peng, L., Li, R. M., Wang, C., and Li, Z. Y.: Emission Characteristics of Volatile Organic Compounds from Typical Coal Utilization Sources: A Case Study in Shanxi of Northern China, #N/A, 21, 15, 10.4209/aaqr.210050, 2021.

- Yang, S., Zhu, B., Shi, S., Jiang, Z., Hou, X., An, J., and Xia, L.: Vertical Features of Volatile Organic Compounds and Their Potential Photochemical Reactivities in Boundary Layer Revealed by In-Situ Observations and Satellite Retrieval, #N/A, 16, 1403, 2024.
- Zhang, Q., Wu, L., Fang, X., Liu, M., Zhang, J., Shao, M., Lu, S., and Mao, H.: Emission factors of volatile organic compounds (VOCs) based on the detailed vehicle classification in a tunnel study, Sci. Total Environ., 624, 878-886, https://doi.org/10.1016/j.scitotenv.2017.12.171, 2018.